ACS OMEGA

Open Access

http://pubs.acs.org/journal/acsodf

Article

Ultrahigh-Sensitivity and Damage-Free Detection of Single Nanometer-Sized Particle

Yan Gao,* Hua Jin, Xiao-Wen Zhang,* and Tian-Sheng Liu*

Cite This: *ACS Omega* 2024, 9, 37672−37677

Read Online

ACCESS | Metrics & More | Article Recommendations | Supporting Information

ABSTRACT: In the past decades, various methods, such as chemical sensing, X-ray screening, and spectroscopy, have been employed to detect explosives for environmental protection and national public security. However, achieving ultrahigh sensitivity for detection, which is crucial for some practical applications, remains challenging. This study employs scanning transmission electron microscopy and electron energy loss spectroscopy (STEM−EELS) to detect individual ∼200 nm explosive nanoparticles of octahydro-1,3,5,7-tetranitro-1,3,5,7-tetrazocine (HMX). The vibrational modes of HMX were acquired for each single nanoparticle under the aloof STEM−EELS mode, which ensures damage-free detection. Detailed comparisons with Raman and infrared spectra validate the acquired data's origin. This work highlights STEM−EELS as an effective tool in explosives detection, offering ultrahigh sensitivity, damage-free, and nanometer spatial resolution, with potential applications in environmental protection, public security, and criminal investigations.

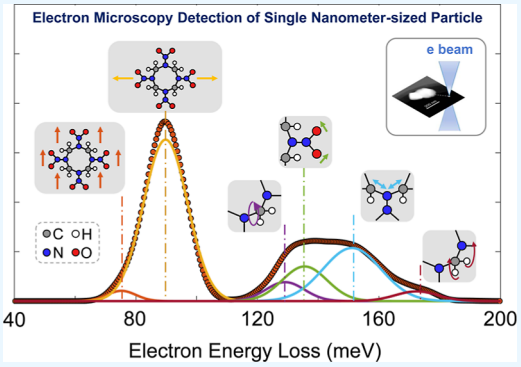

INTRODUCTION

High-sensitivity and reliable detection of explosives is of paramount importance in the fields of environmental protection, national public security, counter-terrorism, stability maintenance, and criminal investigation (e.g., forensic science).[1−7] Over the past decades, various detection methods have been reported.[8−19] They can be mainly cataloged as chemical detection,[11,13,15−17] X-ray screening,[10] gas detection,[8,12] and spectroscopy.[3,9,14,18] Specifically, for chemical detection, chemical sensors are used to detect the specific chemical composition of explosives, including recently developed nanoparticle sensors based on metal oxide semiconductor.[11] For X-ray screening, the objects are scanned by X-ray to detect the possible explosives.[10] Specific gases would be released from the explosives. Thus, by analyzing the gas composition in the air, the explosive can be detected and identified.[8,12] The signature nature of explosives can be also identified through various spectroscopic techniques, such as infrared-spectroscopy,[20] neutron and gamma-ray spectroscopy,[14] and Raman spectroscopy.[9] Note that each of these detection methods has its own advantages and disadvantages (see the details in the Supporting Information). For instance, spectroscopic approaches display very high sensitivities and selectivities but are often expensive and require specialized equipment.[6] X-ray methods offer good sensitivity, but they also typically require necessitate equipment.[10] Gas detection and chemical detection are both convenient and cost-effective methods, but they remain vulnerable to environmental factors.[11]

Particularly, surface-enhanced Raman spectroscopy (SERS) is a widely employed technique in the detection of various materials.[21,22] It has proven to be effective in detecting explosives when inspecting ammunition stockpiles or verifying the composition of explosives. However, in specific applications where the detection of a tiny number of explosives is required, that is, identifying and analyzing the residues at crime scenes such as explosive devices, postblast debris, or suspicious materials, the sensitivity of SERS become insufficient. In fact, not only Raman spectroscopy but also other traditional spectroscopies share similar weakness. To date, ultrahigh sensitivity detection of explosives (e.g., to detect a single particle with nanometer-size), which is highly desirable for some practical applications, is still lacking to best of our knowledge.

The sensitivity of spectroscopies mainly relies on the interaction cross-section between matter and the probing source (e.g., X-ray, laser, neutron). In this sense, electron scattering spectroscopy is expected to achieve higher sensitivity, as the cross-section of electron interaction is typically 10^4 to 10^6 times larger than that of lasers and X-ray, and even much larger than that of neutrons, thanks to the

Received: March 4, 2024
Revised: June 18, 2024
Accepted: July 9, 2024
Published: August 27, 2024

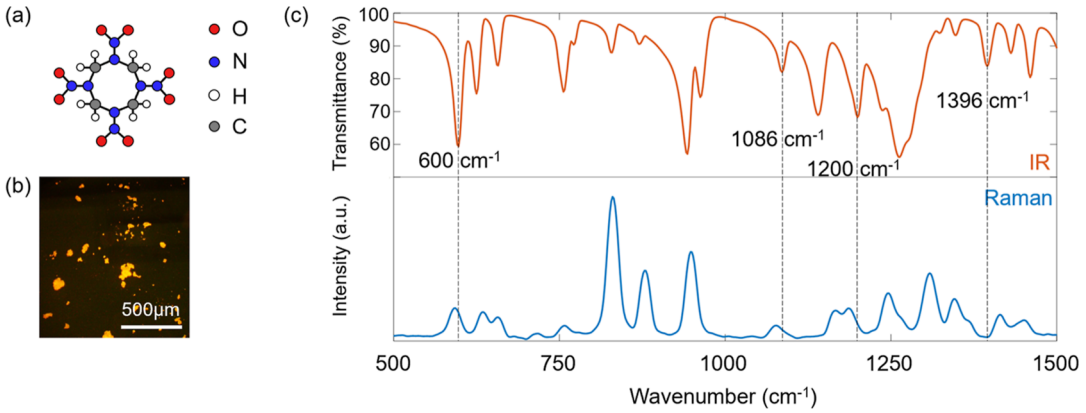

Figure 1. (a) Molecular structure of HMX. Oxygen atoms, nitrogen atoms, hydrogen atoms, and carbon atoms are labeled as red, blue, white, and gray solid cycles. (b) Morphology of HMX powder under optical microscope. The bright parts in the image are HMX powder. (c) FTIR spectrum and Raman spectrum of HMX powder. The dash vertical lines display the peak position observed in the EEL spectrum.

strong Coulomb interactions between the electron and target matter. Recent advances in electron energy loss spectroscopy in scanning transmission electron microscope (STEM−EELS) have enabled meV energy resolution,[23−28] which is sufficient to detect the vibrational properties of chemical bonds, similar to infrared absorption spectroscopy and Raman spectroscopy. Moreover, the aloof configuration for data acquisition allows us to probe organic matter without causing damage.[24] This configuration involves positioning the electron beam in a vacuum far away from the sample without physical contact to avoid direct collision with high-energy electrons. Such a method offers the potential to detect a small number of explosives.

RESULTS AND DISCUSSIONS

In this work, we aim to demonstrate such a capability of the aloof beam EELS configuration to detect a single nanoparticle of explosive with a size of approximately 200 nm. We chose octahydro-1,3,5,7-tetranitro-1,3,5,7-tetrazocine, commonly known as HMX, as an example. HMX is renowned for its exceptional properties, including high detonation velocity, sensitivity to initiation, and outstanding thermal stability. As a result, it holds immense value as a crucial component in various explosive formulations. For instance, HMX plays a pivotal role in the formulation of plastic bonded explosives, which are composite materials where HMX particles are embedded within a polymer matrix.[6] With its extensive use in explosive devices, the development of effective techniques for HMX detection has become a matter of utmost importance.[2]

To ascertain the origin of the acquired EELS data, we compared the signals of a single HMX nanoparticle detected by aloof beam EELS with the Raman and infrared spectra, which showed excellent agreement between the EELS and the infrared spectral data. Additionally, we conducted quantitative analysis of the intensity attenuation in aloof beam EELS with increasing distance away from the tiny HMX particles to achieve an optimized balance between damage-free and signal-to-noise ratio (SNR). Our study unambiguously demonstrates the ability to identify a single ∼200 nm HMX nanoparticle by the STEM−EELS. This opens a new door for ultrahigh sensitivity detection of explosives, particularly in scenarios demanding the identification of minute particles for security and forensic investigations.

The molecular structure of HMX is illustrated in Figure 1a. It consists of a central carbon atom (C) connected to four nitrogen atoms (N) and four oxygen atoms (O). The nitrogen atoms are parts of the tetrazole rings, while the oxygen atoms are associated with the nitro functional groups. Our HMX particles were synthesized using a similar method to that described in previous studies[29] (details in Methods section). We first employed optical microscopy to characterize the morphology of the HMX particles, as depicted in Figure 1b. The particles were placed on a glass slide, which contributes to the dark green background. To investigate the vibrational properties of HMX particles, we conducted measurements using Fourier transform infrared spectroscopy (FTIR) and Raman spectroscopy, as shown in Figure 1c. The spectrum features are in excellent agreement with previous studies.[20] The dashed lines represent the peaks extracted in STEM−EELS for comparison, which are discussed in detail below.

To demonstrate the noncontact detection capabilities of STEM−EELS for HMX particles, we utilized the aloof beam EELS configuration, as depicted in Figure 2a. The STEM high angle annular dark field (HAADF) image (Figure 2b) displays a typical HMX particle with a size of approximately 200 nm situated on a holey carbon film. This positioning allows the e-beam (indicated by the blue color) to pass through a vacuum away from the sample side and the distance can be precisely and easily controlled. Figure 2c presents an EEL spectrum recorded away from the particle (∼260 nm in distance), and the spectral peak positions were fitted using simple Gaussian peak fitting. Under these experimental conditions, dipole scattering dominates, resulting in peak positions (Figure 2c) that closely match several IR spectrum peaks (Table 1). The Raman spectrum of the sample is also plotted in Figure 2c for comparison. Note that the Raman spectrum shows different spectral features because it has different section role than the IR spectrum and STEM−EELS.[30] Schematic representations of these vibrational modes are shown in Figure 2d, based on the previous research.[20]

As the electron beam moves away from the particle, the signal intensity decreases. Figure 3a,b provides detailed intensity variations of the EEL spectra at a set of distance points, where different colors label different positions and their corresponding EEL spectra. It is noteworthy that vibrational signals can still be detected even with a probe positioned 200 nm from the specimen. It becomes increasingly challenging to

https://doi.org/10.1021/acsomega.4c02127
ACS Omega 2024, 9, 37672−37677

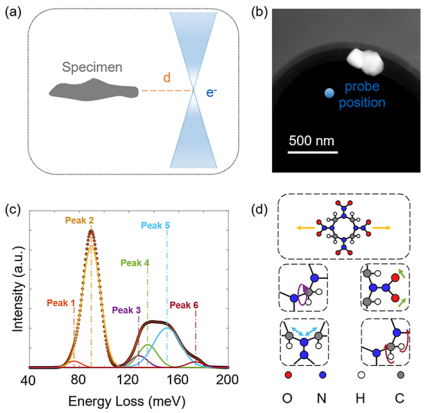

Figure 2. (a) Schematic of the aloof beam EELS configuration: the electron probe is positioned at a distance d away from the sample in the vacuum. The distance is typically from tens to hundreds of nanometers. (b) STEM-HAADF image of a typical HMX particle. (c) The corresponding vibrational EEL spectra of the HMX particle shown in (b) with the electron beam located at the blue point. Several peak positions are labeled by different color dashed lines. (d) Graphs of vibrations corresponding to peaks in (c). Peak 1 (orange) and peak 2 (yellow) are both from the ring deformations, as shown in top panel. Peak 3 (purple) is from the torsions of CH_2, as shown in the left part of the middle panel. Peak 4 (green) is from the rocking of NNO_2, as shown in the right part of the middle panel. Peak 5 (cyan) is from the stretching of NCN, as shown in left part of bottom panel. Peak 6 (crimson) is from the waggling of CH_2, as shown in the right part of the bottom panel.

Table 1. Cross-Reference Table of Peak Positions and Vibrational Modes[a]

serial number	peak positions in EELS (meV)	peak positions in infrared spectra (meV)	vibrational mode
1	76	75	ring deformation
2	91	92	ring deformation
3	127.5	127	CH_2 torsion
4	135.5	136	NNO_2 rock
5	151	151	NCN stretch
6	174	174	CH_2 waggle

[a]The cross-reference table between the peak positions fitted in EEL spectra and corresponding peak positions in the IR spectrum. The first column is the number of the peak positions sorted by their energy values. The second and third columns represent the energy values of the corresponding peak positions in EELS and IR, respectively. The last column represents the molecular vibration modes corresponding to these peaks.

detect very small particles due to the trade-off between the beam-damage and SNR, that is, in order to obtain sufficient SNR for smaller particles, a smaller distance and longer acquisition time are required, and thus larger damage happens. Nevertheless, we have obtained sufficient signal for a smaller HMX nanoparticle (~100 nm) with the same detection distance of 200 nm (details in Figure S2). By carefully inspecting the relation between intensity and distance, we find that beyond tens of nanometers from the specimen, the intensity variation aligns well with the modified Bessel function of second kind (K_0), as described by classical dielectric theory.[24] The intensity and distance are fitted using the aforementioned function, as shown in Figure 3c. Please note that the shape of the fitting function is related to the size, shape of the specimen, and the incident-electron speed.[24]

For HMX particles, we also found notable differences between the EEL spectra obtained under the aloof beam configuration and the infrared spectrum. These disparities result from the distinct spatial scales of detection in these two techniques. The EEL spectra under aloof beam configuration are contributed by the molecular vibrations from a specified tiny HMX particle with specific direction (Figure 2). It is noteworthy that an angle exists between the electric field induced by the electron beam and the polarization direction of the vibration of HMX molecules, which contributes to the variation in peak intensity for different vibrations.[31] More specifically, the differential scattering cross section of the electron is determined by the imaginary part of the dielectric tensor and the scattering vector.[24] Due to the anisotropy of the dielectric tensor in HMX nanoparticles, the probability of electron scattering varies as the scattering vector changes.[24] Therefore, for a specific HMX nanoparticle, it can only contribute a vibrational signal along a certain direction, that is, with the vibration direction perpendicular to the electron beam. As a result, the EEL spectra of a smaller HMX nanoparticle (~100 nm) in Figure S2 show that some different vibrational modes are active compared to the larger nanoparticle (Table S1). In contrast, the infrared spectrum is derived from the average vibrations from numerous HMX particles with various orientations, encompassing contributions from vibrations along all directions.

The spatial resolution of STEM−EELS measurement can easily achieve subnanometer resolution, which is controlled by the high voltage, convergence angle, and aberrations of the electron microscope with aberration corrector. Higher voltage, larger convergence angle, and smaller aberrations can lead to an improvement in spatial resolution, allowing finer details of the sample to be resolved. However, this enhancement comes at the cost of increased damage and reduced signal intensity in aloof beam EEL spectra. In our investigation, the signal of molecular vibrations we observed is primarily contributed by the dipole scattering of incident electrons, which generally has a relatively large cross-section and significant delocalization effect. Hence, the spatial resolution is not critical, and the signal intensity is usually strong enough for detection. On the other hand, although high-energy electrons can easily damage the specimen under traditional TEM characterizations, the aloof configuration can substantially reduce the damage or even achieve completely damage-free detection by simply controlling the distance between the probe and specimen.[24] These unique advantages make aloof beam STEM−EELS a good general method for detecting explosives, especially for those cases with amounts below the limit for other detection methods. However, it also should be pointed out that the limited energy resolution of STEM−EELS (typically ~10 meV in our experiments) may make the molecular vibration modes with similar energies challenging to distinguish.

In summary, our research showcases the potential of STEM−EELS experiments on a single tiny HMX particle, demonstrating its effectiveness in detecting molecular vibrations with ultrahigh sensitivity and high spatial resolution. Although a trade-off exists among the spatial resolution, signal intensity, and damage, we believe that the benefits of using STEM−EELS in the study of these nanometer-sized particles outweigh the limitations. Considering that the energy resolution of the STEM−EELS can readily achieve sub-10

https://doi.org/10.1021/acsomega.4c02127
ACS Omega 2024, 9, 37672−37677

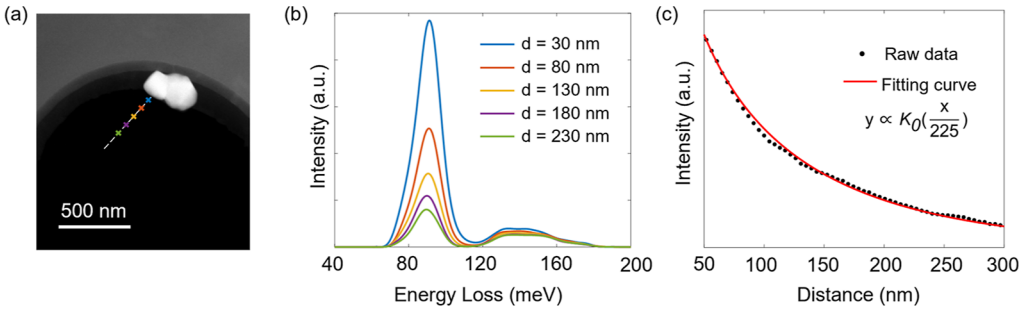

Figure 3. (a) STEM−HAADF image of the same HMX particle in Figure 2. (b) Selected typical spectra showing the spectrum evolution when the probe is moving closer to the specimen; i.e., the intensity becomes higher when the distance is smaller. The corresponding positions are labeled by different colors in (a). (c) Variation of total intensity of EELS signal as the probe away from the sample. The fitting function is also plotted with a red solid line for comparison. The fitted parameter is labeled.

meV nowadays, which is sufficient to detect many vibration signals in molecules, we believe such a measurement capability opens up new possibilities for advanced explosives analysis, contributing to the broader field of environmental protection, public security, and criminal investigation.

METHODS

Synthesis. To prepare HMX, five raw materials, namely, ulotropine, acetic acid, acetic anhydride, ammonium nitrate, and nitric acid, were used. First, ulotropine and acetic acid were prepared into black vinegar solution, ammonium nitrate and nitric acid were prepared into ammonium acid solution, and then black vinegar solution, ammonium acid solution, and acetic anhydride were fed in three ways to react.

EELS Acquiring. The vibrational spectra and HAADF images were acquired at a Nion U-HERMES200 electron microscope equipped with both the monochromator and the aberration corrector operated at 60 kV. The probe convergence semiangle was 10 mrad, and the collection semiangle was 25 mrad. The energy dispersion channel was set as 0.5 meV with 2048 channels in total. The spatially resolved EEL spectra were originally recorded as a spectrum image, with single exposures of 600 ms per pixel. The acquired spectrum images are 220 × 180 nm with 5 nm per pixel.

EELS Processing. All acquired EEL spectra were processed using the Gatan Microscopy Suite and custom-written MATLAB code. The EEL spectra were first aligned by normalized cross-correlation. Next, the block-matching and three-dimensional filtering algorithms were applied to remove Gaussian noise.

For the vibrational spectra, the background arising from both the tail of ZLP and noncharacteristic phonon losses was fitted using the modified Peason-VII function with two fitting windows and then subtracted to obtain the vibrational signal. The Lucy−Richardson algorithm was then employed to ameliorate the broadening effect caused by finite energy resolution, taking the elastic ZLP as the point spread function. The vibrational spectra were fitted using a simple Gaussian peak-fitting model to extract the peak position. And the relation between intensity and distance is fitted by a modified Bessel function of the second kind.

Detailed Comparison among Different Detection Methods. Chemical detection's pros:

1 High sensitivity: Chemical tests can detect trace amounts of explosives.
2 Portable: Some chemical detection kits are compact and easy to carry.

Chemical detection's cons:

1 False positives: Some common substances (e.g., fertilizers) may trigger false alarms.
2 Limited range: Chemical tests are effective only at close distances.

Chemical detection's applicable scenes:
Airports, checkpoints, and public events.
X-ray screening's pros:

1 Noninvasive: X-rays can penetrate objects to reveal hidden items.
2 Wide coverage: Scans entire bags or packages.

X-ray screening's cons:

1 Cost and maintenance: X-ray machines are expensive to install and maintain.

X-ray screening's applicable scenes:
Airports, seaports, and mail facilities.
Gas detection's pros:

1 Rapid response: Gas sensors can detect explosives quickly.
2 Continuous monitoring: Can be used in high-risk areas.

Gas detection's cons:

1 False alarms: Environmental factors (e.g., humidity) may cause false positives.
2 Calibration and maintenance: Sensors require regular checks.

Gas detection's applicable scenes:
Underground transportation is critical infrastructure.
Spectroscopy's pros:

1 High specificity: Identifies unique molecular signatures.
2 Noncontact: No physical sampling required.
3 Versatility: Can analyze various materials.

Spectroscopy's cons:

1 Expensive equipment: Spectrometers can be costly.
2 Skill-dependent: Requires trained operators.

Spectroscopy's applicable scenes:
Laboratories, research facilities, and forensic analysis.

ASSOCIATED CONTENT

Supporting Information

The Supporting Information is available free of charge at https://pubs.acs.org/doi/10.1021/acsomega.4c02127.

Details in experimental setups, including sample synthesis, EELS acquiring and EELS processing, the SAED

https://doi.org/10.1021/acsomega.4c02127
ACS Omega 2024, 9, 37672−37677

pattern, the EEL spectra and corresponding analysis of smaller nanoparticles (PDF)

AUTHOR INFORMATION

Corresponding Authors

Yan Gao − *School of Information and Network Security, People's Public Security University of China, Beijing 100038, China*; Email: gaoyan0718@ppsuc.edu.cn

Xiao-Wen Zhang − *Electron Microscopy Laboratory, School of Physics, Peking University, Beijing 100871, China*; orcid.org/0009-0004-8827-1039; Email: zhangphy1999@stu.pku.edu.cn

Tian-Sheng Liu − *School of Environment and Safety Engineering, North University of China, Taiyuan 030051, China*; Email: liutsh66@sina.com

Author

Hua Jin − *School of Information and Network Security, People's Public Security University of China, Beijing 100038, China*

Complete contact information is available at: https://pubs.acs.org/10.1021/acsomega.4c02127

Notes

The authors declare no competing financial interest.

ACKNOWLEDGMENTS

This work was supported by Double First-Class Innovation Research Project for People's Public Security University of China [no. 2023SYL08]. The authors acknowledge the use of facilities from the Electron Microscopy Laboratory and the helpful discussions with the lab staff.

REFERENCES

(1) Khatua, S.; Goswami, S.; Biswas, S.; Tomar, K.; Jena, H. S.; Konar, S. Stable multiresponsive luminescent MOF for colorimetric detection of small molecules in selective and reversible manner. *Chem. Mater.* **2015**, *27* (15), 5349−5360.

(2) Hu, Z.; Deibert, B. J.; Li, J. Luminescent metal-organic frameworks for chemical sensing and explosive detection. *Chem. Soc. Rev.* **2014**, *43* (16), 5815−5840.

(3) Tabrizchi, M.; Ilbeigi, V. Detection of explosives by positive corona discharge ion mobility spectrometry. *J. Hazard. Mater.* **2010**, *176* (1−3), 692−696.

(4) Wang, C.; Huang, H.; Bunes, B. R.; Wu, N.; Xu, M.; Yang, X.; Yu, L.; Zang, L. Trace detection of RDX, HMX and PETN explosives using a fluorescence spot sensor. *Sci. Rep.* **2016**, *6*, 25015.

(5) Xie, Z.; Ge, H.; Du, J.; Duan, T.; Yang, G.; He, Y. Compartmentalizing incompatible tandem reactions in pickering emulsions to enable visual colorimetric detection of nitramine explosives using a smartphone. *Anal. Chem.* **2018**, *90* (19), 11665−11670.

(6) Caygill, J. S.; Davis, F.; Higson, S. P. Current trends in explosive detection techniques. *Talanta* **2012**, *88*, 14−29.

(7) Geng, Y.; Ali, M. A.; Clulow, A. J.; Fan, S.; Burn, P. L.; Gentle, I. R.; Meredith, P.; Shaw, P. E. Unambiguous detection of nitrated explosive vapours by fluorescence quenching of dendrimer films. *Nat. Commun.* **2015**, *6*, 8240.

(8) Walsh, M. E. Determination of nitroaromatic, nitramine, and nitrate ester explosives in soil by gas chromatography and an electron capture detector. *Talanta* **2001**, *54* (3), 427−438.

(9) Gaft, M.; Nagli, L. UV gated Raman spectroscopy for standoff detection of explosives. *Opt. Mater.* **2008**, *30* (11), 1739−1746.

(10) Yang, Y.; Li, Y.; Wang, H.; Li, T.; Wu, B. Explosives detection using photoneutrons produced by X-rays. *Nucl. Instrum. Methods Phys. Res., Sect. A* **2007**, *579* (1), 400−403.

(11) Gui, Y.; Xie, C.; Xu, J.; Wang, G. Detection and discrimination of low concentration explosives using MOS nanoparticle sensors. *J. Hazard. Mater.* **2009**, *164* (2−3), 1030−1035.

(12) Calderara, S.; Gardebas, D.; Martinez, F. Solid phase micro extraction coupled with on-column GC/ECD for the post-blast analysis of organic explosives. *Forensic Sci. Int.* **2003**, *137* (1), 6−12.

(13) Holmgren, E.; Carlsson, H.; Goede, P.; Crescenzi, C. Determination and characterization of organic explosives using porous graphitic carbon and liquid chromatography-atmospheric pressure chemical ionization mass spectrometry. *J. Chromatogr. A* **2005**, *1099* (1−2), 127−135.

(14) Farahmand, M.; Boston, A. J.; Grint, A. N.; Nolan, P. J.; Joyce, M. J.; Mackin, R. O.; D'Mellow, B.; Aspinall, M.; Peyton, A. J.; van Silfhout, R. Detection of explosive substances by tomographic inspection using neutron and gamma-ray spectroscopy. *Nucl. Instrum. Methods Phys. Res., Sect. B* **2007**, *261* (1−2), 396−400.

(15) Meaney, M. S.; McGuffin, V. L. Investigation of common fluorophores for the detection of nitrated explosives by fluorescence quenching. *Anal. Chim. Acta* **2008**, *610* (1), 57−67.

(16) Jimenez, A. M.; Navas, M. J. Chemiluminescence detection systems for the analysis of explosives. *J. Hazard. Mater.* **2004**, *106* (1), 1−5.

(17) Singh, S. Sensors-an effective approach for the detection of explosives. *J. Hazard. Mater.* **2007**, *144* (1−2), 15−28.

(18) Gottfried, J. L.; De Lucia, F. C., Jr.; Munson, C. A.; Miziolek, A. W. Laser-induced breakdown spectroscopy for detection of explosives residues: a review of recent advances, challenges, and future prospects. *Anal. Bioanal. Chem.* **2009**, *395* (2), 283−300.

(19) Gaurav; Kaur, V.; Kumar, A.; Malik, A. K.; Rai, P. K. SPME-HPLC: a new approach to the analysis of explosives. *J. Hazard. Mater.* **2007**, *147* (3), 691−697.

(20) Puiu, A.; Giubileo, G.; Nunziante Cesaro, S. Vibrational spectrum of HMX at CO_2 laser wavelengths: a combined DRIFT and LPAS study. *Int. J. Spectrosc.* **2012**, *2012*, 1−4.

(21) Heleg-Shabtai, V.; Zaltsman, A.; Sharon, M.; Sharabi, H.; Nir, I.; Marder, D.; Cohen, G.; Ron, I.; Pevzner, A. Explosive vapour/particles detection using SERS substrates and a hand-held Raman detector. *RSC Adv.* **2021**, *11* (42), 26029−26036.

(22) Guven, B.; Eryilmaz, M.; Üzer, A.; Boyaci, I. H.; Tamer, U.; Apak, R. Surface-enhanced Raman spectroscopy combined with gold nanorods for the simultaneous quantification of nitramine energetic materials. *RSC Adv.* **2017**, *7* (59), 37039−37047.

(23) Krivanek, O. L.; Lovejoy, T. C.; Dellby, N.; Aoki, T.; Carpenter, R. W.; Rez, P.; Soignard, E.; Zhu, J.; Batson, P. E.; Lagos, M. J.; et al. Vibrational spectroscopy in the electron microscope. *Nature* **2014**, *514* (7521), 209−212.

(24) Rez, P.; Aoki, T.; March, K.; Gur, D.; Krivanek, O. L.; Dellby, N.; Lovejoy, T. C.; Wolf, S. G.; Cohen, H. Damage-free vibrational spectroscopy of biological materials in the electron microscope. *Nat. Commun.* **2016**, *7*, 10945.

(25) Lagos, M. J.; Trugler, A.; Hohenester, U.; Batson, P. E. Mapping vibrational surface and bulk modes in a single nanocube. *Nature* **2017**, *543* (7646), 529−532.

(26) Haiber, D. M.; Crozier, P. A. Nanoscale probing of local hydrogen heterogeneity in disordered carbon nitrides with vibrational electron energy-loss spectroscopy. *ACS Nano* **2018**, *12* (6), 5463−5472.

(27) Hachtel, J. A.; Huang, J.; Popovs, I.; Jansone-Popova, S.; Keum, J. K.; Jakowski, J.; Lovejoy, T. C.; Dellby, N.; Krivanek, O. L.; Idrobo, J. C. Identification of site-specific isotopic labels by vibrational spectroscopy in the electron microscope. *Science* **2019**, *363* (6426), 525−528.

(28) Jokisaari, J. R.; Hachtel, J. A.; Hu, X.; Mukherjee, A.; Wang, C.; Konecna, A.; Lovejoy, T. C.; Dellby, N.; Aizpurua, J.; Krivanek, O. L.; et al. Vibrational spectroscopy of water with high spatial resolution. *Adv. Mater.* **2018**, *30*, No. e1802702.

(29) Zhang, Y.; Xu, Z.; Zhang, L.; Zhang, G.; He, D.; Wang, X.; Ruan, J.; Zhang, D.; Jin, G.; Ma, X.; et al. Investigation of the key active intermediate for the synthesis of 1,3,5,7-tetranitro-1,3,5,7-tetraazacyclooctane: hydrolysis and nitrolysis of 1-acetoxymethyl-3,5,7-trinitro-1,3,5,7-tetraazacyclooctane. *Energ. Mater. Front.* **2020**, *1* (2), 67−73.
(30) Silberman, E.; Morgan, H. W. Use of group theory in the interpretation of infrared and Raman spectra. [Tables, vibrational spectroscopy]; *ORNL/TM-5666; TRN: 77−006876*; United States, 1977. https://www.osti.gov/biblio/7329949. https://www.osti.gov/servlets/purl/7329949. .
(31) Radtke, G.; Taverna, D.; Menguy, N.; Pandolfi, S.; Courac, A.; Le Godec, Y.; Krivanek, O. L.; Lovejoy, T. C. Polarization selectivity in vibrational electron-energy-loss spectroscopy. *Phys. Rev. Lett.* **2019**, *123* (25), 256001.

https://doi.org/10.1021/acsomega.4c02127
ACS Omega 2024, 9, 37672−37677